

GRB 011121: A collimated outflow into wind-blown surroundings¹

J. Greiner^{1,2}, S. Klose³, M. Salvato^{1,2}, A. Zeh³, R. Schwarz^{1,4}, D.H. Hartmann⁵, N. Masetti⁶, B. Stecklum³, G. Lamer¹, N. Lodieu¹, R.D. Scholz¹, C. Sterken⁷, J. Gorosabel^{8,9}, I. Burud⁹, J. Rhoads⁹, I. Mitrofanov¹⁰, M. Litvak¹⁰, A. Sanin¹⁰, V. Grinkov¹⁰, M.I. Andersen¹, J.M. Castro Cerón¹¹, A.J. Castro-Tirado^{8,12}, A. Fruchter⁹, J.U. Fynbo¹³, J. Hjorth¹⁴, L. Kaper¹⁵, C. Kouveliotou¹⁶, E. Palazzi⁶, E. Pian¹⁷, E. Rol¹⁵, N.R. Tanvir¹⁸, P.M. Vreeswijk¹⁹, R.A.M.J. Wijers¹⁵, E. van den Heuvel¹⁵

¹ *Astrophysikalisches Institut, 14482 Potsdam, Germany*

² *Max-Planck-Institut für extraterrestrische Physik, 85741 Garching, Germany*

³ *Thüringer Landessternwarte Tautenburg, 07778 Tautenburg, Germany*

⁴ *Universitäts-Sternwarte Göttingen, Geismarlandstr. 11, 37083 Göttingen, Germany*

⁵ *Clemson University, Department of Physics and Astronomy, Clemson, SC 29634, USA*

⁶ *Istituto di Astrofisica Spaziale e Fisica Cosmica, CNR, Sez. di Bologna, Via Gobetti 101, 40129 Bologna, Italy*

⁷ *University of Brussels (VUB), Pleinlaan 2, 1050 Brussels, Belgium*

⁸ *Instituto de Astrofísica de Andalucía (IAA-CSIC), P.O. Box 03004, 18080 Granada, Spain*

⁹ *Space Telescope Science Institute, 3700 San Martin Drive, Baltimore, MD 21218, USA*

¹⁰ *Space Research Institute, Profsoyusnaya 84/32, 117810 Moscow, Russia*

¹¹ *Real Instituto y Observatorio de la Armada, Sección de Astronomía, 11.110 San Fernando-Naval (Cádiz), Spain*

¹² *Laboratorio de Astrofísica Espacial y Física Fundamental, Madrid, Spain*

¹³ *Department of Physics and Astronomy, University of Aarhus, Ny Munkegade, 8000 Aarhus C, Denmark*

¹⁴ *Astronomical Observatory, University of Copenhagen, Juliane Maries Vej 30, 2100 Copenhagen, Denmark*

¹⁵ *University of Amsterdam, Kruislaan 403, 1098 SJ Amsterdam, The Netherlands*

¹⁶ *NSSTC, SD-50, 320 Sparkman Drive, Huntsville, AL 35805, U.S.A.*

¹⁷ *INAF, Osservatorio Astronomico di Trieste, Via Tiepolo 11, 34131 Trieste, Italy*

¹⁸ *Department of Physical Sciences, Univ. of Hertfordshire, College Lane, Hatfield Herts, AL10 9AB, UK*

¹⁹ *European Southern Observatory, Alonso de Cordova 3107, Vitacura, Casilla 19001, Santiago 19, Chile*

ABSTRACT

We report optical and near-infrared follow-up observations of GRB 011121 collected predominantly at ESO telescopes in Chile. We discover a break in the afterglow light curve after 1.3 days, which implies an initial jet opening angle of about 9° . The jet origin of this break is supported by the fact that the spectral energy distribution is achromatic during the first four days. During later phases, GRB 011121 shows significant excess emission above the flux predicted by a power law, which we interpret as additional light from an underlying supernova. In particular, the spectral energy distribution of the optical transient approximately 2 weeks after the burst is clearly not of power-law type, but can be presented by a black body with a temperature of ~ 6000 K. The deduced parameters for the decay slope as well as the spectral index favor a wind scenario, i.e. an outflow into a circum-burst environment shaped by the stellar wind of a massive GRB progenitor. Due to its low redshift of $z=0.36$, GRB 011121 has been the best example for the GRB-supernova connection until GRB 030329, and provides compelling evidence for a circum-burster wind region expected to exist if the progenitor was a massive star.

Subject headings: gamma rays: bursts — techniques; photometric — supernovae: general

1. Introduction

In the presently favoured scenario for classical gamma-ray bursts (GRBs), occurring at cosmological distances (measured redshift range so far $0.36 < z < 4.5$; van Paradijs et al. 1997; Andersen et al. 2000), the explosion of a very massive star leads to a fireball and a short, beamed flash of gamma-rays (Woosley 1993; Fryer et al. 1999; Mészáros 2002), resulting in three physically distinct observational phenomena, namely the GRB itself, a long-lasting afterglow and the classical supernova (SN) light. Whereas the afterglow emission is probably fed by the kinetic energy of the collimated, relativistic outflow, the supernova light is caused by the decay of radioactive nuclei created and released during the stellar explosion. The maximum of the supernova light is expected at $\sim 10\text{--}20(1+z)$ days after the explosion, though at present it is not clear whether or not the GRB and the supernova explosion are delayed (Vietri & Stella 1998). One of the basic consequences of this hypernova scenario is that it predicts (and links) the occurrence of a GRB with a jet, the unavoidable strong wind from the massive progenitor star, and the supernova light (Heger et al. 2003).

Earlier evidence on the GRB-SN connection was initially based on the coincidence of GRB 980425 and SN1998bw (Galama et al. 1998), and subsequently some supernova light contribution was found in the late-time light curves of GRB 980326 (Castro-Tirado & Gorosabel 1999, Bloom et al. 1999), GRB 970228 (Galama et al. 2000), GRB 970508 (Sokolov et al. 2002) and possibly GRB 980703 (Holland et al. 2001), GRB 990712 (Björnsson et al. 2001), GRB 991208 (Castro-Tirado et al. 2001) and GRB 000911 (Lazzati et al. 2001).

Observations of massive stars in our Galaxy have shown that they lose matter via strong stellar winds in the LBV and in the Wolf-Rayet evolutionary phase. GRB progenitors are expected to be very massive stars and perhaps physically related to Ib/c supernovae (Heger et al. 2003). The progenitors of these stars should develop fast winds at the end of their lives and thus, wind features

¹Based on observations collected at the European Southern Observatory, La Silla and Paranal, Chile (ESO Programme 165.H-0464).

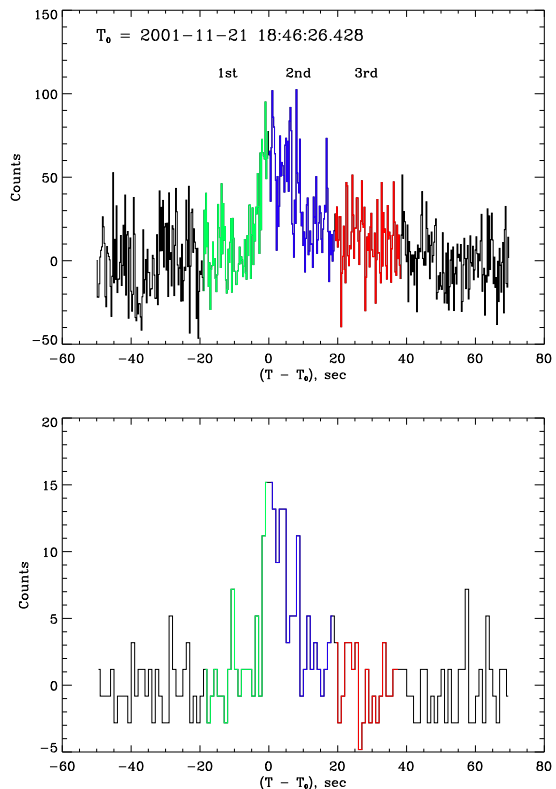


Fig. 1.— Light curve of GRB 011121 as recorded by HEND on Mars Odyssey in the outer scintillator at >30 keV with 0.25 sec time resolution (top) and in the inner scintillator at >60 keV with 1 sec time resolution (bottom). The time axis zero point (UT) is indicated at the top. The three colours represent the three successive time segments used for the spectral fitting (see Fig. 2).

are expected to be seen in afterglow light curves. The evolution of classical supernova remnants into wind-blown bubbles has been a target of detailed investigations since years (e.g., Benetti et al. 1999; Landecker et al. 1999). What has been missing in GRB research until GRB 030329 (Hjorth et al. 2003), however, was a strong observational link between an underlying supernova component in an afterglow light curve and evidence for a fireball expanding into a stellar wind profile. Significant work into this direction has been done over the past years by many groups from the theoretical as well as from the observational side (e.g., Mészáros, Rees, & Wijers 1998; Chevalier & Li

2000) and GRBs with wind-profile interactions have been identified in some cases, including GRB 980425/SN 1998bw (Chevalier & Li 2000). However, if one excludes GRB 980425 from this list, prior to GRB 011121 the observational data base was rather poor. The burst 011121 changed this observational situation, though in a less spectacular way than GRB 030329. Not only was the distance of the burster relatively small but also the light curve steepened 1 day after the burst so that a bright supernova component became visible.

GRB 011121 was detected by the GRBM/WFC onboard BeppoSAX on 2001 November 21, 18:47:21 UT and localized to initially 5 arcmin (Piro 2001a). Subsequent analysis refined this position to 2 arcmin accuracy (Piro 2001b), and the triangulation of the GRB arrival times as measured by Ulysses, BeppoSAX (Hurley et al. 2001) and HEND (Hurley et al. 2002) further refined the coordinates. A follow-up X-ray observation with the BeppoSAX narrow-field instruments revealed a fading X-ray afterglow (Piro et al. 2001).

Follow-up optical/NIR observations of GRB 011121 were quickly started by several groups, leading to independent discoveries of the afterglow (e.g., Wyrzykowski et al. 2001; Greiner et al. 2001). Further observations revealed a rather small distance, $z \approx 0.36$ (Infante et al. 2001), and excess emission above the early power-law decay (Garnavich et al. 2001). The interpretation of this excess light as a possible supernova bump attracted much attention and resulted in the so far best sampling of GRB afterglow emission at late times.

Here we report the results of observations obtained by the GRACE² (GRB Afterglow Collaboration at ESO) consortium.

2. Observations

2.1. X-rays/Gamma-rays

The light curves of GRB 011121 measured with the two detectors of HEND are shown in Fig. 1. Integrated into the Third Interplanetary Network, the “Mars Odyssey” satellite has two instruments with GRB detection capabilities: the Gamma-Ray Spectrometer and the High Energy Neutron Detector (HEND). HEND combines four detectors

to measure the spectra of neutrons and gamma-rays (Mitrofanov et al. 2003). In particular, the inner/outer CsI-scintillators can measure gamma-ray photons in the 30–1000 keV range, at commandable integration times, and in case of a GRB-trigger (or solar flare), time histories at 1.0/0.25 sec resolution are recorded.

Fig. 1 shows that the gamma-ray emission is characterized by a main peak with ~ 10 sec duration, followed by a ~ 20 sec tail. Thus, GRB 011121 clearly belongs to the long-duration subclass of GRBs.

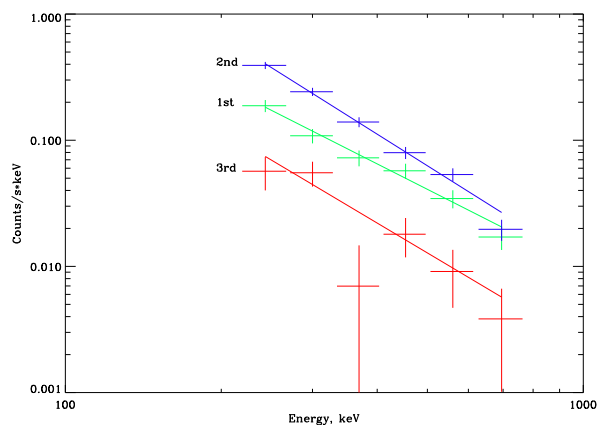


Fig. 2.— Energy spectra of GRB 011121 above 200 keV, as recorded by HEND on Mars Odyssey in the outer scintillator for three successive time segments, shown as green, blue and red in the light curve (see Fig. 1.)

According to the HEND energy spectra (Fig. 2) there is no obvious spectral evolution along the light curve of GRB 011121. All three 20 sec segments of the time profile have spectra with the same power law slope with a photon index of -2.35 ± 0.25 (after backwards folding of the model with the instrument response). There is no evidence in the HEND data that the early afterglow emission started already at the time of the last segment of the burst.

Based on the power law spectral slope of 2.35, the fluence is $2 \pm 0.4 \times 10^{-5}$ erg cm^{-2} in the 250–700 keV range. This corresponds to an (isotropic) energy release of $E = 2.7 \times 10^{52}$ erg at the given redshift (luminosity distance of 2.07 Gpc) and the cosmological parameters $\Omega_{\Lambda} = 0.7$, $\Omega_M = 0.3$, and

²<http://zon.wins.uva.nl/~grb/grace/>

$H_0 = 65 \text{ km s}^{-1} \text{ Mpc}^{-1}$.

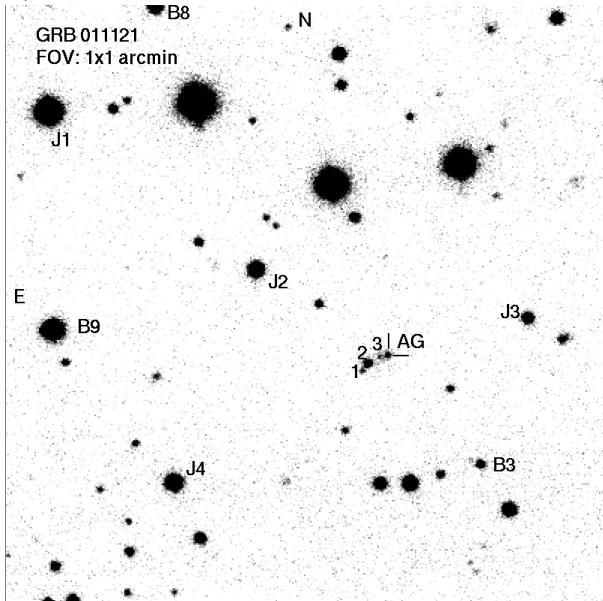


Fig. 3.— *J* band finding chart of GRB 011121 obtained on 2001 Nov. 24 with ISAAC/VLT. Marked are the afterglow (AG), neighbouring objects (1, 2), the host galaxy (3) and some local standards (J1–J4, B3, B8, B9).

2.2. Optical and NIR Imaging

About 9 hours after the GRB, K_s - and R -band images were obtained at La Silla (ESO) with SOFI (equipped with a 1024×1024 HgCdTe HAWAII array with $18.5 \mu\text{m}$ pixels and a plate scale of $0''.29/\text{pixel}$) at the 3.58m NTT, and with EFOSC2 (equipped with a 2048×2048 thinned Loral/Lesser CCD with $15 \mu\text{m}$ pixels and a plate scale of $0''.157/\text{pixel}$) at the 3.6m telescope, respectively. After our independent discovery of the afterglow, second epoch observations plus some exposures with additional filters were obtained (~ 4 hrs later) at the end of that night. Multi-colour photometry continued at the NTT and 3.6m telescope during the next three days and at the VLT thereafter. Due to the rapidly decreasing afterglow brightness we switched to the instruments at the 8.2m Very Large Telescopes (VLT) starting on day 3 after the GRB. For our near-infrared (NIR) observations, the short wavelength ($0.9\text{--}2.5 \mu\text{m}$) arm of the infrared spectrometer ISAAC (equipped with a 1024×1024

pixel Rockwell HgCdTe array and a plate scale of $0''.147/\text{pixel}$) on the VLT-telescope Antu was used, and for the optical observations the Focal Reducer and Spectrograph FORS (equipped with a SITE CCD with $24 \mu\text{m}$ pixels and a plate scale of $0''.2/\text{pixel}$) at VLT/Yepun.

Additional imaging was performed in the R and I bands at the ESO 1.54m Danish telescope on La Silla (Chile), in the H band at the Anglo-Australian Telescope (AAT) and in the J and H bands at the 4-m Blanco telescope of the Cerro Tololo Interamerican Observatory (CTIO). The 1.54m Danish telescope was equipped with a 2048×4096 EEV/MAT frame-transfer CCD (illuminated area is 2048×2048 pixel) with $15 \mu\text{m}$ pixels, which provides a plate scale of $0''.39/\text{pixel}$. At the AAT the IRIS2 instrument with a 1024×1024 Rockwell HAWAII-1 HgCdTe detector was used, having a pixel scale of $0''.446/\text{pixel}$. At CTIO, the Ohio State InfraRed Imager/Spectrometer (OSIRIS) with a 1024×1024 HAWAII-1 HgCdTe detector was used, having a plate scale of $0''.161/\text{pixel}$.

2.3. Spectroscopy

Spectroscopic observations were performed during the first two days in several wavelength bands to derive the redshift and during the maximum of the late-time bump to search for signatures of the potential supernova and to derive host galaxy parameters. In the JK bands the short-wavelength arm of ISAAC was used at low resolution (with a final dispersion of $3.6 \text{ \AA}/\text{pixel}$ in the J band, and $7.2 \text{ \AA}/\text{pixel}$ in the K band), The $1''.0$ slit was used. The JK band spectra were both taken at $1''.2$ seeing, thus giving a FWHM resolution of 29 \AA (J band) and 59 \AA (K band).

Optical spectra were taken with FORS2 at the Yepun telescope at three different occasions, each with a different grism (see Tab. 1). The 150I grism has a mean $5.5 \text{ \AA}/\text{pixel}$ scale, which at the $0''.5$ seeing and the use of a $0''.7$ slit led to a resolution of 14 \AA (FWHM). Grism 300I has a mean $2.59 \text{ \AA}/\text{pixel}$ scale, leading to a resolution of 13 \AA (FWHM) at $0''.7\text{--}1''.2$ seeing and use of the $1''.0$ slit. Finally, grism 600B with a mean $1.2 \text{ \AA}/\text{pixel}$ scale at $1''.2\text{--}1''.5$ seeing and the $1''.0$ slit led to a FWHM resolution of 6 \AA . The pixel scale changes by less than 5% from the red to the blue end of each grism. The peak spectral response for the

Table 1: Log of the observations

Date (UT)	Telescope/Instrument	Filter/Grism ^(a)	Exposure (sec)	Seeing	Brightness (mag) ^(b)
2001 Nov 22 03:03–03:25	ESO NTT/SOFI	K_S	10×63	0''7	15.19±0.07
2001 Nov 22 04:03–04:14	ESO 3.6 m/EFOSC2	R_C	3×180	1''5	18.86±0.02
2001 Nov 22 07:30–08:01	ESO 3.6 m/EFOSC2	R_C	3×600	1''0	19.51±0.01
2001 Nov 22 07:47–08:22	ESO NTT/SOFI	J	25×70	0''8	17.47±0.04
2001 Nov 22 08:23–08:47	ESO NTT/SOFI	H	17×70	0''7	16.72±0.05
2001 Nov 22 08:47–09:06	ESO NTT/SOFI	K_S	13×70	0''9	16.09±0.07
2001 Nov 22 14:00–14:14	AAO AAT/IRIS2	H	10×60	2''7	17.30±0.25
2001 Nov 23 00:04–00:20	ESO NTT/SOFI	K_S	11×70	1''2	17.71±0.10
2001 Nov 23 00:20–00:39	ESO NTT/SOFI	J	13×70	1''6	19.38±0.10
2001 Nov 23 04:30–04:40	ESO 3.6 m/EFOSC2	R_C	3×180	(c)	21.23±0.05
2001 Nov 23 04:41–04:57	ESO 3.6 m/EFOSC2	B	3×300	(c)	22.40±0.50
2001 Nov 23 04:58–05:08	ESO 3.6 m/EFOSC2	V	3×180	(c)	21.95±0.15
2001 Nov 23 08:29–08:45	ESO NTT/SOFI	J	11×70	0''9	19.73±0.10
2001 Nov 23 08:45–09:01	ESO NTT/SOFI	K_S	11×70	0''9	18.29±0.10
2001 Nov 23 08:29–08:39	ESO 3.6 m/EFOSC2	R_C	3×180	1''3	21.75±0.08
2001 Nov 23 08:39–08:44	ESO 3.6 m/EFOSC2	B	300	1''6	>21.70
2001 Nov 23 06:45–08:34	ESO Yepun/FORS2	600B	2×2400+1500	1''5, 1''0, 1''2	—
2001 Nov 23 07:22–08:34	ESO Antu/ISAAC	1.1–1.4 μm	3600	1''2	—
2001 Nov 24 06:24–06:48	ESO Antu/ISAAC	K_S	15×60	0''7	19.30±0.08
2001 Nov 24 06:53–07:16	ESO Antu/ISAAC	H	15×60	0''7	19.81±0.05
2001 Nov 24 07:18–07:36	ESO Antu/ISAAC	J_S	10×90	0''6	20.93±0.10
2001 Nov 24 07:53–08:59	ESO Antu/ISAAC	1.95–2.55 μm	3600	1''2	—
2001 Nov 24 07:43–08:01	ESO Yepun/FORS2	B	3×300	0''8	23.70±0.30
2001 Nov 24 08:02–08:14	ESO Yepun/FORS2	V	3×180	0''8	23.37±0.05
2001 Nov 24 08:15–08:27	ESO Yepun/FORS2	R_{special}	3×180	0''8	22.93±0.08
2001 Nov 25 06:43–06:59	ESO Antu/ISAAC	J_S	10×90	0''9	21.64±0.30
2001 Nov 25 07:01–07:24	ESO Antu/ISAAC	H	15×60	0''6	20.73±0.10
2001 Nov 25 07:27–07:52	ESO Antu/ISAAC	K_S	15×60	0''8	20.02±0.10
2001 Nov 25 06:34–08:10	ESO Yepun/FORS2	150I	3×1800	0''5	—
2001 Nov 25 08:10–08:22	ESO Yepun/FORS2	R_{special}	3×180	0''8	23.68±0.15
2001 Nov 25 08:23–08:34	ESO Yepun/FORS2	V	3×180	(d)	>24.40
2001 Nov 25 07:41–08:13	ESO 1.54 m Danish	R_C	1880	1''1	23.60±0.40
2001 Nov 30 08:05–08:51	CTIO OSIRIS	H	19×60	0''7	>19.40
2001 Dec 01 08:07–08:39	CTIO OSIRIS	J	8×120	0''9	>20.10
2001 Dec 03 07:50–08:25	CTIO OSIRIS	J	10×120	1''2	>20.10
2001 Dec 05 06:28–07:01	ESO Melipal/FORS1	V	3×600	0''9	24.30±0.02
2001 Dec 05 07:02–07:33	ESO Melipal/FORS1	R_C	3×600	0''9	23.20±0.08
2001 Dec 05 07:34–08:07	ESO Melipal/FORS1	I_C	3×600	0''9	22.35±0.25
2001 Dec 05 06:53–08:09	ESO Antu/ISAAC	J_S	40×90	0''6	22.41±0.15
2001 Dec 07 06:45–08:02	ESO Antu/ISAAC	J_S	40×90	0''6	22.69±0.10
2001 Dec 08 06:20–06:30	ESO Melipal/FORS1	V	600	0''8	24.09±0.02
2001 Dec 09 06:49–08:05	ESO Antu/ISAAC	J_S	40×90	0''7	22.52±0.15
2001 Dec 09 07:33–07:43	ESO Melipal/FORS1	V	600	1''0	23.94±0.02
2001 Dec 10 06:47–06:57	ESO Melipal/FORS1	R_C	600	0''8	23.65±0.08
2001 Dec 11 07:33–08:06	ESO Melipal/FORS1	R_C	3×600	0''6	23.45±0.08
2001 Dec 11 08:07–08:29	ESO Melipal/FORS1	V	2×600	0''7	24.18±0.02
2001 Dec 12 05:12–07:30	ESO Yepun/FORS2	300I	4×1800	0''7–1''2	—
2001 Dec 13 07:19–08:46	ESO Antu/ISAAC	J_S	40×90	0''7	22.89±0.15
2001 Dec 15 05:10–05:27	ESO 1.54m Danish	I_C	4×900	1''2	>24.70
2001 Dec 16 04:51–05:08	ESO 1.54m Danish	I_C	2×900	1''3	>23.90
2001 Dec 17 04:55–05:12	ESO 1.54m Danish	I_C	4×900	2''0	>23.80
2001 Dec 17 07:20–08:47	ESO Antu/ISAAC	J_S	40×90	1''0	22.79±0.30
2001 Dec 18 04:45–05:01	ESO 1.54m Danish	I_C	2×900	1''1	>23.80
2002 Feb 09 04:04–05:24	ESO Antu/ISAAC	J_S	40×90	0''5	>24.85

(a) The R_{special} filter is about 10% broader than the standard R_C . Filters J_S and K_S are narrower with respect to the canonical J and K bands, respectively: J_S has a width of 0.16 μm (instead of 0.29 μm), and K_S has a width of 0.29 μm centered at 2.16 μm (instead of 0.35 μm centered at 2.20 μm). However, since both narrow-band filters have a higher transmission than the canonical filters, the net effect is that $J - J_S \lesssim 0.05$ ($K - K_S \lesssim 0.02$) when comparing the ISAAC J_S vs. the SOFI J filter. The grisms 150I, 300I and 600B are described in the text.

(b) Not corrected for Galactic foreground extinction.

(c) Image quality affected by guiding problems.

(d) Variable seeing due to varying cirrus.

150I, 300I and 600B grism is at 5000 Å, 7500 Å and 4000 Å, respectively.

Table 2: Local photometric B, V standards

Star	Coordinates (J2000.0)	B	V
B1	11 ^h 34 ^m 18 ^s .9 -76°01'37"	20.11±0.01	18.93±0.01
B2	11 ^h 34 ^m 19 ^s .7 -76°02'06"	20.95±0.01	19.95±0.02
B3	11 ^h 34 ^m 27 ^s .2 -76°01'52"	22.93±0.03	21.93±0.04
B4	11 ^h 34 ^m 27 ^s .2 -76°02'34"	23.94±0.07	22.49±0.05
B5	11 ^h 34 ^m 27 ^s .4 -76°02'22"	21.58±0.01	20.35±0.02
B6	11 ^h 34 ^m 29 ^s .9 -76°02'36"	23.69±0.05	22.27±0.05
B7	11 ^h 34 ^m 33 ^s .3 -76°01'33"	20.64±0.01	19.59±0.01
B8	11 ^h 34 ^m 36 ^s .2 -76°01'07"	23.00±0.05	21.41±0.04
B9	11 ^h 34 ^m 38 ^s .9 -76°01'38"	20.37±0.01	19.03±0.01
B10	11 ^h 34 ^m 41 ^s .9 -76°01'04"	25.25±0.16	23.01±0.09
B11	11 ^h 34 ^m 52 ^s .9 -76°01'31"	23.50±0.05	21.57±0.03

B4=R5, B6=R6, B7=J2.

Table 3: Local photometric R_c, I_c standards

Star	Coordinates (J2000.0)	R_c	I_c
R1	11 ^h 34 ^m 10 ^s .8 -76°02'50"	20.87±0.05	20.06±0.02
R2	11 ^h 34 ^m 11 ^s .2 -76°03'23"	20.96±0.02	20.35±0.02
R3	11 ^h 34 ^m 15 ^s .4 -76°00'37"	19.97±0.04	19.34±0.01
R4	11 ^h 34 ^m 18 ^s .0 -76°02'32"	23.43±0.10	22.95±0.08
R5	11 ^h 34 ^m 27 ^s .2 -76°02'34"	21.75±0.04	21.09±0.03
R6	11 ^h 34 ^m 29 ^s .9 -76°02'36"	21.48±0.04	20.80±0.03
R7	11 ^h 34 ^m 33 ^s .3 -76°02'30"	21.82±0.06	21.13±0.03
R8	11 ^h 34 ^m 40 ^s .8 -76°02'36"	20.47±0.03	19.98±0.01
R9	11 ^h 34 ^m 41 ^s .9 -76°01'35"	22.36±0.05	21.84±0.05
R10	11 ^h 34 ^m 43 ^s .8 -76°01'27"	22.78±0.07	21.49±0.04
R11	11 ^h 34 ^m 45 ^s .4 -76°01'32"	19.36±0.08	18.87±0.01

R5=B4, R6=B6.

3. Data reduction, analysis, and basic results

3.1. Photometry

The optical and near-infrared images were reduced in standard fashion using IRAF³ as well as

³IRAF is distributed by the National Optical Astronomical Observatories, which is operated by the Associated Universities for Research in Astronomy, Inc., under contract to the National Science Foundation.

ESO's *eclipse* package (Devillard 2002). Photometric calibration of the GRB field was performed using SExtractor (Bertin & Arnouts 1996). Airmass correction was done according to the coefficients provided by ESO's Web pages (in units of mag airmass⁻¹): $k_B = 0.240 \pm 0.007$, $k_V = 0.112 \pm 0.005$, $k_R = 0.091 \pm 0.007$, $k_I = 0.061 \pm 0.006$ for VLT FORS1 and FORS2, and $k_J = 0.06$, $k_H = 0.06$, $k_K = 0.07$ for VLT ISAAC at Paranal, $k_B = 0.20$, $k_V = 0.11$, $k_R = 0.05$, $k_I = 0.02$ for La Silla. For the optical observations, the Landolt standard fields observed were SA 92-249, MarkA, Rubin 152, GD 108 and SA 100. For the NIR calibration the UKIRT infrared standard star FS 12 was used.

Local photometric standards (Tables 2, 3, 4) were selected according to their detection in $BVRI$ by SExtractor and a small scatter in their measured magnitudes on the images taken at different observing epochs. Moreover, care was taken that the difference between the deduced Bessel- R band magnitudes (FORS1) and the R_{special} magnitudes (FORS2) of these stars was less than about 0.1 mag. These local photometric standards were then used to derive the magnitude of the optical transient (Tab. 1) after removal of the host galaxy.

The accuracy of the photometry in the different filters has been cross-checked on the set of images taken on 24 November 2001 via a comparison of the observed stellar brightnesses versus those of expected synthetic stars. For this we have first measured the magnitudes of our local standard stars using YODA (Drory 2003), after having convolved the images to the common worst seeing of 1".4. In a second step, we took synthetic stellar spectra from the Pickles spectral library and convolved those with the filter transmission curves and efficiencies of the corresponding instrument (FORS2+ISAAC). Finally, we overplotted the measured standards over the synthetic stars in various color-color diagrams (Fig. 5). This shows that the photometric calibration is of coherent quality over all the 7 filter bands used.

3.2. The light curve

GRB 011121 occurred at galactic coordinates $(l_{\text{II}}, b_{\text{II}}) = 297.77, -12.43$. The Schlegel, Finkbeiner, & Davis (1998) extinction maps predict $E(B - V) = 0.46$ mag along this line of sight through the Galaxy. Assuming the usual ratio

Table 4: Local photometric standards for the NIR bands (Fig. 3)

Star	Coordinates (J2000.0)	J_s	H	K_s
J1	11 ^h 34 ^m 39 ^s .0 -76°01'17"	15.21±0.05	14.81±0.05	14.91±0.05
J2	11 ^h 34 ^m 33 ^s .3 -76°01'33"	17.28±0.05	16.74±0.05	16.82±0.05
J3	11 ^h 34 ^m 25 ^s .8 -76°01'37"	18.56±0.05	18.28±0.05	18.27±0.05
J4	11 ^h 34 ^m 35 ^s .6 -76°01'53"	17.15±0.05	16.31±0.05	16.31±0.05

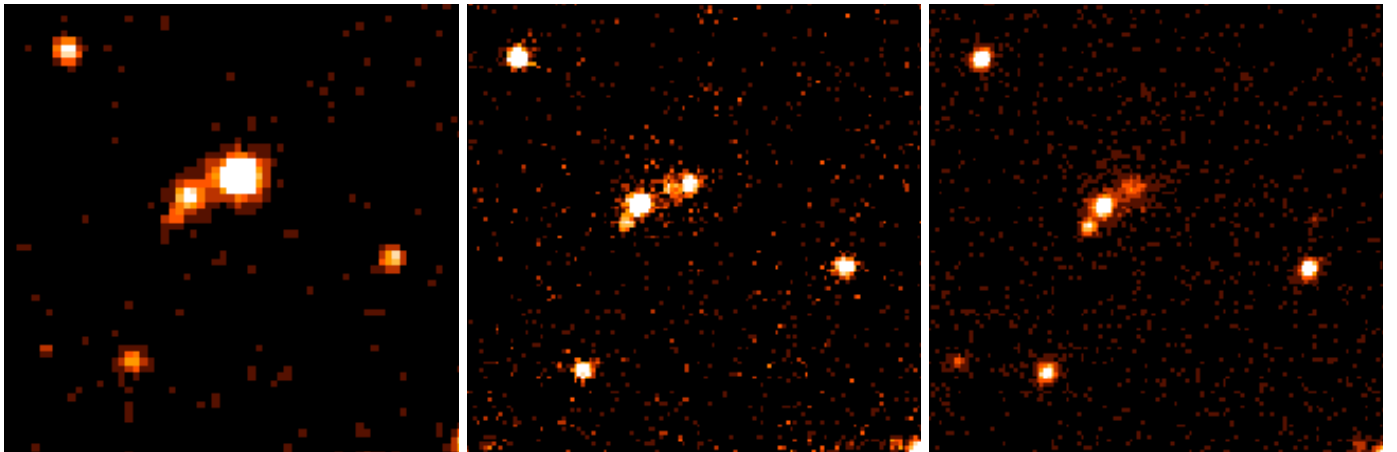


Fig. 4.— Sequence of J band images of GRB 011121 taken with SOFI/NTT on 22 November 2001 (left), and with VLT/ISAAC on 24 November 2001 (middle) and 9 February 2002 (right). The right-most image clearly shows the host galaxy (labeled #3 in Fig. 3), whereas the GRB afterglow has disappeared. The field is $17'' \times 17''$, North at the top and East to the left.

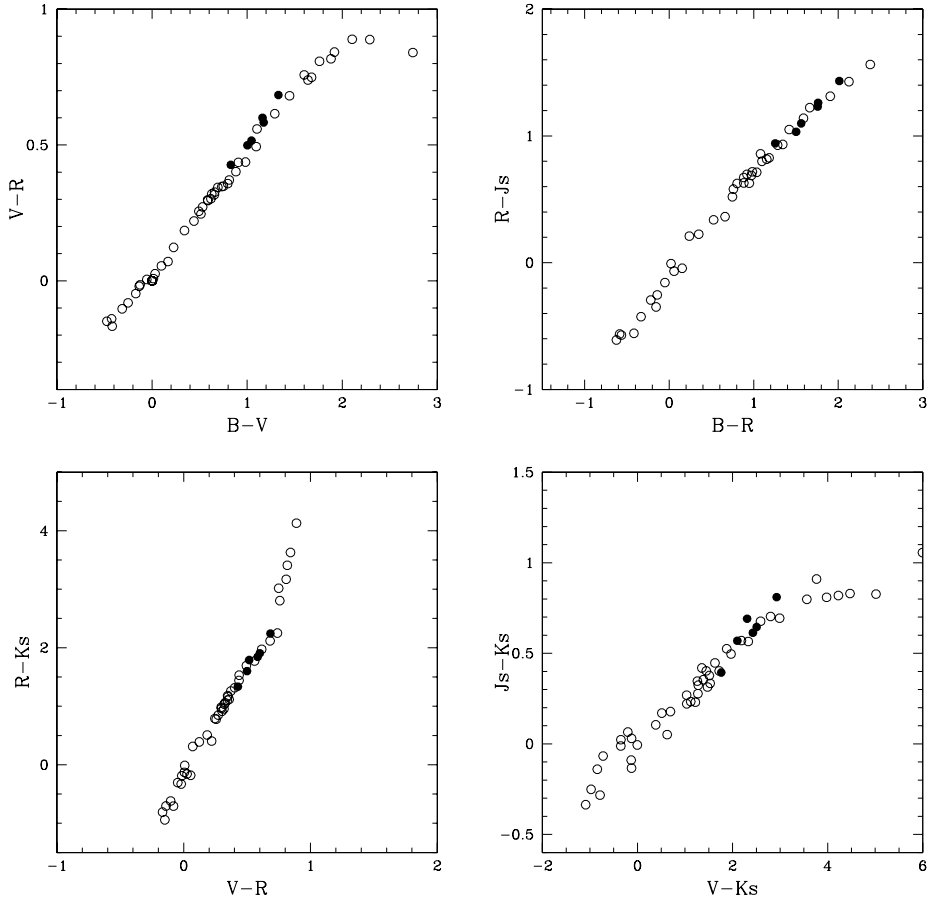


Fig. 5.— Color-color diagrams of bright, non-saturated stars detected in the central area of the images of GRB 01121 (filled circles), compared with the expected color-color sequence as derived from the convolution of the stellar library of Pickles with the total filter efficiency curves of the instruments used (open circles).

of visual-to-selective extinction of 3.1, this gives $A_V \approx 1.4$ mag. The HI maps of Dickey & Lockman (1990) give $N_{\text{H}} = 1.2 \times 10^{21} \text{ cm}^{-2}$ which translates into $A_V \approx 0.9$ mag using the extinction to absorption correlation of Predehl & Schmitt (1995). We used the higher of the above two values, and then followed standard procedures (Rieke & Lebofsky 1985; Cardelli, Clayton, & Mathis 1989; Reichart 2001) to calculate the extinction in the other photometric bands, resulting in: $A_B = 1.87$ mag, $A_{R_c} = 1.15$ mag, $A_{I_c} = 0.83$ mag, $A_J = 0.40$ mag, $A_H = 0.25$ mag and $A_{K_s} = 0.17$ mag. In all the light curve plots this extinction has been corrected for.

Accurate photometry of the afterglow requires a careful removal of contaminating light from the

underlying GRB host galaxy which has an angular extent of two arcseconds (Fig. 4). This was accomplished with a two-component intensity profile model, as described in more detail in §4.4. The model is derived from the J band image of 9 February 2002, taken at a seeing of $0''.45$. We assume that the radial profile of the host galaxy is the same in all filter bands, as justified by a comparison of the scale lengths of 86 face-on galaxies in the B, V, R, H filter bands by de Jong (1996), who finds that they are identical within the errors (the disk scale length ratio of R vs. H band is 1.07 ± 0.08). The subtraction is done in count space on the images before the photometry, and for each image the host model is first convolved with the seeing of that exposure, and then itera-

tively adjusted in intensity until the area around the afterglow is best matched to the undisturbed background somewhat further away. As a consistency test we computed the host magnitude for each image taking into account the seeing convolution and the final intensity normalization, and found that the host magnitude differs at most by 0.07 mag (two instances) from the values given in §4.4. In addition, star 1 from Fig. 3 has been used to monitor the quality of the subtraction, which was always accurate to better than 0.05 mag. This ensures that the light curve shape is not contaminated by this subtraction procedure. An example of the result is shown in Fig. 6.

3.2.1. Light curve based on observations prior to $t = 10$ days

Figure 7 shows the afterglow light curve in the R_c -band after removal of the flux from the underlying host galaxy, and after correcting for galactic extinction. Theoretical fits were obtained with the formula of Beuermann et al. (1999) in the representation of Rhoads & Fruchter (2001):

$$F_\nu(t) = 2^{1/n} F_\nu(t_b) [(t/t_b)^{\alpha_1 n} + (t/t_b)^{\alpha_2 n}]^{-1/n}. \quad (1)$$

Here F_ν is the flux density, t_b the break time (in days), and n the parameter which describes the smoothness of the break. In all cases we fitted apparent magnitudes. Here and in the following we use the standard notation for the time and frequency dependence of the flux density in the simple fireball model: $F_\nu \propto t^{-\alpha} \nu^{-\beta}$.

The fit of the R_c -band data excluding the measurements at $t \geq 10$ days gives an early-time slope of $\alpha_1 = 1.62 \pm 0.62$, a late-time slope of $\alpha_2 = 2.44 \pm 0.38$, and a break time $t_b = 1.2 \pm 1.0$ days ($\chi^2/\text{d.o.f.} = 0.45$; d.o.f. \equiv degrees of freedom). The parameter n which measures the sharpness of the break, was fixed at $n = 10$, corresponding to a sharp break. However, values as low as $n = 1$ give similarly good fits.

At early times (22 November 2001, 3:30 UT) we measure $R_c - K = 2.7 \pm 0.1$ mag (after correction for galactic extinction). Hence, the spectral slope of the afterglow is $\beta = 0.80 \pm 0.15$. Two days later, on 24 November 2001, 7:00 UT, we find $\beta = 0.62 \pm 0.05$ based on our $BVRJHK$ data, which is consistent with the earlier result, and which is fully in agreement with the results

obtained by Garnavich et al. (2003) and Price et al. (2002). These afterglow parameters are fully consistent with those expected from the simple versions of the fireball as well as observations of previous gamma-ray burst afterglows (e.g., van Paradijs, Kouveliotou, & Wijers 2000).

We can improve the fit by adding more data points as follows. First, using the deduced spectral index of the early afterglow we can estimate that at the time of the single AAO observations (Table 1), i.e. before the deduced break time, the R_c -band magnitude of the optical transient was 20.12 ± 0.25 . Second, we can include in our fit the R -band data from Garnavich et al. (2003) for $t < 0.6$ days. In doing so, we get $\alpha_1 = 1.62 \pm 0.39$, $\alpha_2 = 2.44 \pm 0.34$, $t_b = 1.20 \pm 0.75$ days, $\chi^2/\text{d.o.f.} = 1.11$.

3.2.2. Light curve based on all observations

Including the “late-time” data (after $t = 10$ days) to the fits adds substantially more freedom, since different model components can now compensate each other. As before, we only use R_c -band data for the analysis. In order to account for the excess light after $t = 10$ days, we assume that this “bump” is due to light from an underlying supernova. In fact, it has been officially designated as SN 2001ke (Garnavich et al. 2003). To model this supernova component we employ the observed $UBVR_cI_c$ light curves of SN 1998bw (Galama et al. 1998) as a template.

The effects of the redshift of GRB 011121 ($z=0.36$) were taken into account assuming the cosmological parameters as given in section 2.1. For SN 1998bw we used a redshift of $z = 0.0085$ (Tinney et al. 1998). The entire numerical procedure is in detail explained in Zeh & Klose (2003). It interpolates smoothly between the $UBVRI$ light curves of SN 1998bw (Galama et al. 1998)⁴, so that for any given time a set of flux densities is calculated. The predicted time-dependent supernova light curve of a redshifted GRB-supernova based on the SN 1998bw template is then calculated according to the procedure outlined by Dado et al. (2002a). The apparent magnitude of a redshifted SN 1998bw in a given photometric band is finally obtained by integrating over the flux densities (transformed into per unit wavelength),

⁴see also <http://zon.wins.uva.nl/titus/grb980425.html>

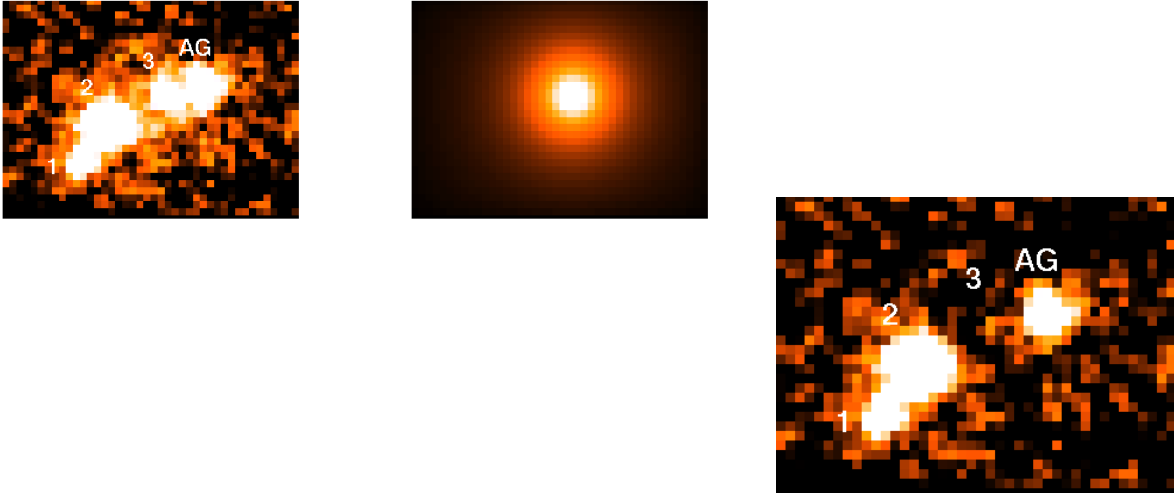


Fig. 6.— Sequence of R band sub-images of 24 Nov. 2001 showing the original (left), the model of the host galaxy (center) and the host-subtracted image (right). All sub-images are shown at the same scale and with the same cut values. Labels are the same as in Fig. 3. Photometry of the lower-left star in the original and the host-subtracted image has been done for all epochs to ensure that no oversubtraction occurred. The residual scatter in this comparison star was in the range of 0.02–0.05 mag.

multiplied by the corresponding filter response function, and by applying the usual normalization factors. The entire procedure has been successfully applied for GRB 030329/SN 2003dh (Hjorth et al. 2003; Zeh et al. 2003) and has been successfully tested against the results obtained by others for other bursts (e.g., Masetti et al. 2003; Dado et al. 2002a). The results are shown in Figs. 8 and 9.

The resulting parameters are: $\alpha_1 = 1.63 \pm 0.61$, $\alpha_2 = 2.73 \pm 0.45$, $t_b = 1.26 \pm 0.94$ days and $k = 0.85 \pm 0.11$ with $\chi^2/\text{d.o.f.} = 1.11$. Here, k is the luminosity ratio in the R_c band between the GRB 011121 supernova and SN 1998bw at maximum (at $z = 0.36$). As before, the parameter n was held constant at 10 because otherwise the sparse data would not allow convergence of the numerical fitting algorithm. Our conclusions are not sensitive to the exact value of this parameter. On the other hand, we emphasize that the value we get for the parameter k assumes a ‘perfect’ SN 1998bw light curve at the redshift of the burster. Any potential relation between luminosity and light curve shape of a supernova in a certain photometric band is neglected here. In particular, k does not say anything about the bolometric luminosity of the GRB supernova compared to SN

1998bw. This parameter is also sensitive to potential additional parameters which one can introduce in order to improve the fit of the SN light curve (see § 4.2.2).

For SN 1998bw we assumed zero extinction along the line of sight through our Galaxy. Accordingly, our results obtained for the luminosity of the supernova accompanying GRB 011121 in units of the luminosity of SN 1998bw, the parameter k , scale as $k \rightarrow k \times \exp(-A_V(\text{SN 1998bw})/1.086)$, if such an extinction is taken into account. Note also that we assumed a Galactic extinction along the line of sight of $A_V(\text{Gal}) = 1.4$ mag. If smaller values are preferred (Bloom et al. 2002), k has to be corrected/reduced again.

Figures 4 (middle panel), 8 and 9 show that the SN light already affected the afterglow light a few days after the GRB. This implies a substantial impact on the measurement of the parameter α_2 . Unfortunately, due to instrumental constraints, we have a data gap between days 4 and 10 after the burst trigger so that the 1σ error of the deduced α_2 rises substantially when we include the SN light in the fit. Note that most of the data published previously are not host subtracted, and therefore cannot be simply added to our data set (Brown

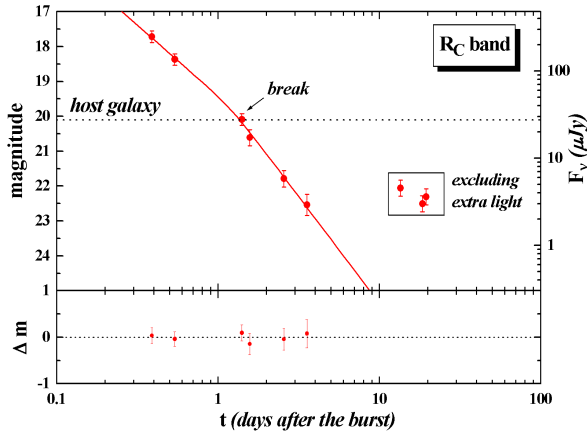


Fig. 7.— R_c -band light curve of the afterglow of GRB 011121 and a fit to the data prior to $t = 10$ days. Compared to Tab. 1a conservative systematic 1σ error of 0.15 mag has been added to all data. The break in the power-law decay occurs at $t_b = 1.2$ days. At late times the afterglow is significantly brighter than predicted by the power-law. Note the particularly bright host galaxy.

et al. 2001; Phillips et al. 2001; Price et al. 2001; Stanek & Wyrzykowski 2001). Despite this added uncertainty, our analysis clearly indicates the presence of a break about one day after the burst. The exact time of the break is sensitive to the details of the fit (compare the results we obtain by fitting data prior to $t = 10$ days vs. fitting all the data), but the existence of the break at $t \sim 1$ day is clearly established. Previous studies of the afterglow light curve of GRB 011121 did not find this break (e.g., Price et al. 2002; Garnavich et al. 2003), which can be attributed to sparse sampling of the afterglow at this particular time. It remains difficult to explain why the radio data of the afterglow do not agree with a jet model (Price et al. 2002).

3.3. The spectrum of the afterglow

The VLT/FORS2 spectrum of the afterglow (including light from the host galaxy and the underlying supernova) contains several strong emission lines (Figs. 10, Tab. 5), but no absorption lines. The redshift determined from these lines is $z = 0.362 \pm 0.001$ (see the figures for line identifications), consistent with results of Infante et al.

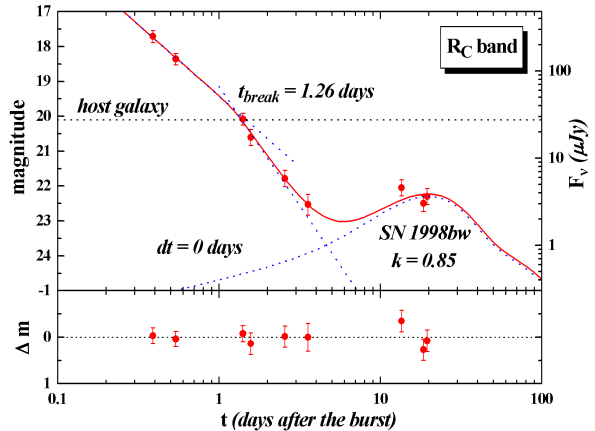


Fig. 8.— R_c -band light curve based on eq. (1) and an additional supernova component, assuming $dt = 0$ days (eq. 2). Note that all photometric data are corrected for Galactic extinction (§3.2). Compared to Tab. 1 a conservative systematic 1σ error of 0.15 mag has been added to all data.

(2001). This redshift corresponds to a luminosity distance of 2.07 Gpc (assuming the cosmological parameters of section 2.1), and a distance modulus of 41.59 mag.

Using the foreground A_V (§3.2), we have determined the extinction values in the lines A^{line} , and corrected the measured line fluxes according to $F_{\text{corr}} = F_{\text{obs}} \times \exp(\tau)$, where $\tau = 1/1.086 \times A^{\text{line}}$ is the continuum extinction according to the galactic A_V .

4. Results and Discussion

4.1. The afterglow model and the $\alpha - \beta$ relations

Since our finding of a jetted explosion is crucial for an understanding of the observational data we have carefully checked this result. When we fit our R_c -band data (Table 1) with a single power-law plus SN component we get $\alpha = 1.98 \pm 0.11$, $k = 0.81 \pm 0.11$ with $\chi^2/\text{d.o.f.} = 1.49$. Not only is the fit worse in comparison to the fit based on the Beuermann equation, the value we now get for α is notably larger (3σ deviation) than the one deduced for the early-time slope of the afterglow light curve (Price et al. 2002; Garnavich et al. 2003). This again points to a change in the fading

Table 5: Measured line fluxes (corrected for galactic extinction) and luminosities.

Line	λ_{obs} (Å)	z	Flux (10^{-16} erg/cm ² /s)	Luminosity (10^{40} erg/s)
OII] 3726	5079	0.363	0.41±0.03	8.6
H β	6625	0.362	0.22±0.04 / 0.14±0.04 ⁽¹⁾	3.2/2.0
OIII] 4963	6760	0.362	0.11±0.06 / 0.08±0.05 ⁽¹⁾	1.6/1.1
OIII] 5007	6821	0.362	0.35±0.05 / 0.16±0.04 ⁽¹⁾	4.9/2.2
H α	8945	0.363	0.96±0.08 / 0.81±0.09 ⁽¹⁾	9.2/7.7
Pa α	25550	0.362	2.58±0.12	14.8

⁽¹⁾ The first number is measured from the 150I spectrum on 25 November 2001, while the second number is measured from the 300I spectrum on 12 December 2001.

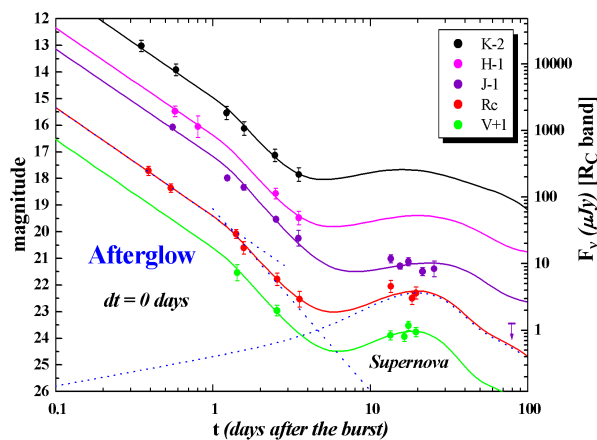


Fig. 9.— The same as Fig. 8 but now showing the best fit in all photometric bands. When fitting the V , J , H , K_s -band light curves the afterglow parameters deduced from the R_c -band fit (α_1 , α_2 , $[n]$, t_b) were used as input, i.e. the functional form of the afterglow light curve was fixed. The supernova light curve (extrapolated towards the H and K bands), however, was calculated for the chosen photometric band.

behavior of the afterglow between about 0.4 and 2 days after the burst. Moreover, our deduced α_1 for the early-time slope of the afterglow light curve is fully consistent with the result obtained by Price et al. (2002) and Garnavich et al. (2003) based on their optical/NIR data. In fact, when we fit their data we confirm that they do not show evidence for a break in the light curve. We attribute this to the lack of data around $t = 1$ day. This makes us confident that the break in the light curve which

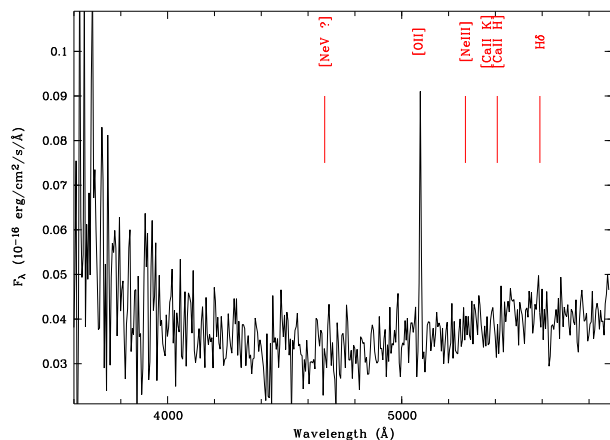


Fig. 10.— Spectrum of GRB 011121 in the blue band, taken on 23 Nov. 2001 with VLT/FORS2 equipped with the 600B grism. While only the [O II] line is detected beyond doubt, we also indicate the positions of other lines which could have been expected.

we deduce based on our observations is a real effect.

In Tab. 6 we list the predicted spectral slope β corresponding to the measured α 's for various afterglow scenarios. Basically, we have to decide here between an ISM and a wind model for a jetted explosion and to constrain the position of the cooling break frequency in the spectral energy distribution (SED) of the afterglow light at the time of the observation. From the comparisons of the predicted β , based on the theoretical $\alpha - \beta$ relations, with the observed one on 22 November 2001, 3:30 UT, and on 24 November 2001, 7:00 UT, we

conclude (see also Fig. 15):

1. The model predictions agree best with the observations for the wind scenario. In this model, the presence of a late “bump” is the natural consequence of the supernova following the stage of rapid mass loss in a massive progenitor star.
2. The data favor the interpretation that during our observations the cooling break frequency ν_c , which separates the contribution of fast-cooling electrons from slow-cooling electrons in the afterglow light (see Sari et al. 1998 for their original definition), was above the optical/NIR bands ($\nu_c \gtrsim 10^{15}$ Hz). This is in agreement with the conclusions drawn by Price et al. (2002) based on their observational data; we refer the reader to this publication for a further discussion of this point.
3. The power-law index p of the electron energy distribution, $N(\gamma_e) d\gamma_e \propto \gamma_e^{-p} d\gamma_e$ was close to the expectations from particle acceleration in relativistic shocks (e.g., Sari et al. 1999).

Within our measurement errors, there is no need for an additional extinction by dust in the GRB host galaxy. A wavelength-dependent extinction by cosmic dust in the GRB host galaxy would tend to increase β , i.e., redden the afterglow light. For example, this was observed in the optical/near-infrared afterglow of GRB 000418 (Klose et al. 2000). The low value of β we and others (Garnavich et al. 2003; Price et al. 2002) find for the afterglow of GRB 011121 however, after correction for the influence of reddening by Galactic dust, compared with various model predictions based on the observed light curve shape (Tab. 6), gives us no strong hint for an additional dust component acting along the line of sight. Grey dust in the GRB host galaxy could still be there (wavelength-independent scattering cross section in the considered photometric bands), but this cannot be deduced from our data.

On the other hand, one should be aware of the fact that the results obtained are sensitive to the adopted Galactic extinction, $A_V(\text{Gal})$, along the line of sight. For example, if we had used $A_V(\text{Gal}) = 0.9$ mag, as it suggested by the H I maps (§ 3.2),

then the extinction corrected β for the intrinsic optical afterglow would have been 1.1, based on our measured $R_c - K$ color of the optical transient on 22 November 2001, 3:30 UT. We favor the higher extinction value (1.4 mag), however. The early multi-color *UBVR**IJK* observations of the GRB afterglow by Garnavich et al. (2002) give a best fit for the Galactic reddening along the line of sight of $E(B - V) = 0.43 \pm 0.07$ mag. For a standard ratio of total-to-selective extinction of 3.1, this is basically consistent with our chosen value for $A_V(\text{Gal})$. We note also that an adopted extinction of $A_V(\text{Gal}) = 1.4$ mag is still consistent with the result deduced by Price et al. (2001) within their claimed 1σ error bar ($A_V(\text{Gal}) = 1.16 \pm 0.25$ mag).

We note that the observed change in the decay slope of the light curve around the break time is in agreement with the predictions of the jet-wind model, provided that the steepening of the light curve is due to the sideways expansion of the jet (Rhoads 1999).

It has been argued (Kumar & Panaitescu 2000) that for an external density profile as r^{-2} the jet break in the light curve is expected to be very gradual, taking at least two decades in time before most of the steepening sets in. In the case of GRB 011121, the break in the light curve is certainly shallower, extending no more than one decade in time (even with fits using $n=1$ the “break” extends only from 0.5–2.5 days, still less than a decade). While this may be considered a problem, more extensive considerations have shown a large diversity of light curve shapes, depending not only on the density profile but also on the evolution of the Lorentz factor, whether jets are uniform or non-uniform, and the difference of viewing and jet angle (e.g., Wei & Jin 2003).

4.2. The supernova and the wind signature

4.2.1. Supernova features

The light curve of GRB 011121 provides the clearest case to date for excess emission above the usual power law extrapolation. The excess in this case appears to become significant about one week after the burst (Fig. 9). This feature has been heralded as strong evidence for a supernova component (Bloom et al. 2002; Dado et al. 2002b; Gar-

Table 6: Predicted β values for various afterglow scenarios. Assuming a relativistic jetted explosion then for observations at $t < t_{\text{break}}$ (pre-break time) the isotropic model holds and $\alpha = \alpha_1$, whereas for $t > t_{\text{break}}$ (post-break time) the jet model applies and $\alpha = \alpha_2$. We use here $\alpha_1 = 1.62 \pm 0.39$ and $\alpha_2 = 2.44 \pm 0.34$ (see § 3.2.1). The parameter s is the power-law index of the density profile of the circumburst medium, $n(r) \propto r^{-s}$. For an ISM model $s = 0$, for a wind model $s = 2$. Case 1 stands for $\nu > \nu_c$, case 2 for $\nu < \nu_c$. In the former case the electron power-law index is given by $p = 2\beta$, whereas in the latter case $p = 2\beta + 1$ (e.g., Sari et al. 1999).

afterglow model	$\beta(\alpha)$	predicted β	electron p
ISM, iso, case 1	$(2\alpha + 1)/3$	1.41 ± 0.26	2.82 ± 0.52
ISM, iso, case 2	$2\alpha/3$	1.08 ± 0.26	3.16 ± 0.52
ISM, jet, case 1	$\alpha/2$	1.22 ± 0.17	2.44 ± 0.34
ISM, jet, case 2	$(\alpha - 1)/2$	0.72 ± 0.17	2.44 ± 0.34
wind, iso, case 1	$(2\alpha + 1)/3$	1.41 ± 0.26	2.82 ± 0.52
wind, iso, case 2	$(2\alpha - 1)/3$	0.75 ± 0.26	2.50 ± 0.52
wind, jet, case 1	$\alpha/2$	1.22 ± 0.17	2.44 ± 0.34
wind, jet, case 2	$(\alpha - 1)/2$	0.72 ± 0.17	2.44 ± 0.34

navich et al. 2003; Price et al. 2002). Garnavich et al. (2003) proposed the supernova label SN 2001ke for this afterglow, although no obvious supernova features were apparent in their Magellan/LDSS2 spectrum obtained on Dec 7, 2001. While it is far from proven that the late emission observed in GRB 011121 is in fact due to a supernova, this interpretation is most natural. If we believe the SN-bump picture, the observations of Garnavich et al. (2003) provide a stern warning: SN1998bw (used in our analysis) may not be appropriate as a “template” for SN-light associated with gamma-ray bursts. Given that to date we have a rather limited sample of supernovae associated with GRBs (see the recent review by Weiler et al. 2002), we are limited in what we can conclude from the bump in the afterglow of GRB 011121, except that it is obvious that the simple afterglow model is unable to explain features like these. Shock rejuvenation and inhomogeneities in the GRB environment or energy injection can explain the kind of bumpy afterglow observed in the case of GRB 021004 (e.g., Lazzati et al. 2002, Holland et al. 2003), but does not account for the long-term (weeks), sustained bump observed in GRB 011121. Supernovae, on the other hand, provide a natural explanation for the energy and also the time scale involved in the late bump we are considering here.

During the maximum of the SN bump (Fig. 13), the observed brightnesses of the afterglow are $J = 22.8 \pm 0.1$, $R = 23.4 \pm 0.1$, and $V = 22.8 \pm 0.1$. This is about 3.6 mag, 3.3 mag, and 3.7 mag fainter than the total light of the host galaxy (see below). Although not all of the host was covered by the slit, the host galaxy still dominated the collected light – even for the spectrum taken on 12 December 2001, around the maximum of the bump. Thus, the lack of any supernova signature in the spectrum is no argument against the supernova interpretation of the bump (Fig. 11), as pointed out by Garnavich et al. (2003).

The extinction-corrected (§3.2) absolute magnitudes for the supernova with a k -correction in the VRJ bands of 0.85 mag (Leibundgut 1990), 0.55 mag and zero, respectively, are $M_J = -19.18$, $M_R = -19.79$, and $M_V = -19.83$. Comparison with the absolute magnitudes of SN 1998bw suggest that the supernova in GRB 011121 is slightly brighter in the V band, but fainter at longer wavelengths.

4.2.2. The GRB-supernova connection

While we use SN 1998bw as a template supernova, we added one degree of freedom to the fitting procedure by allowing for a shift dt of the observed SN maximum (t_{011121}^{max}) with respect to the predicted one for a redshifted SN 1998bw ($t_{1998\text{bw}}^{\text{max}}$),

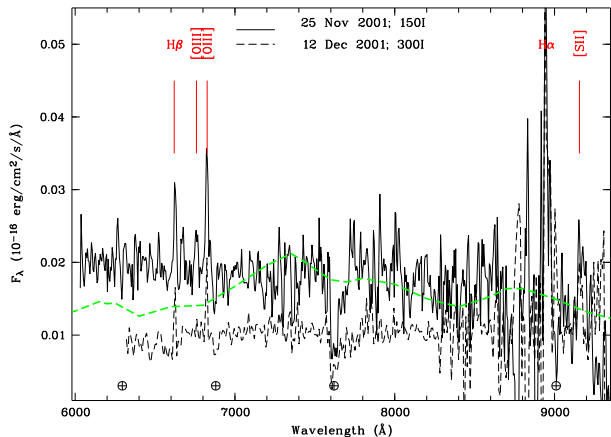


Fig. 11.— Spectrum of GRB 011121 in the red band, taken with VLT/FORS2 equipped with the 150I (25 Nov. 2001, top) and 300I (12 December 2001, bottom; shifted by 0.01 units downwards) grisms, respectively. Some line identifications are indicated. Taking slit losses on 12 December 2001 into consideration, both spectra represent basically the host spectrum, since at the covered wavelength range the afterglow has faded below the brightness of the host. The dashed line shows the spectrum of SN 1998bw 24 days after the maximum (Patat et al. 2001), redshifted to $z=0.36$ and diminished in brightness to 85% (see §3.2.2), thus clearly demonstrating that the supernova was too faint with respect to the host galaxy to be discovered spectroscopically.

i.e.

$$dt = t_{011121}^{\max} - t_{1998bw}^{\max}. \quad (2)$$

With this extra degree of freedom added, the best fit parameters become: $\alpha_1 = 1.67 \pm 0.58$, $\alpha_2 = 3.55 \pm 1.35$, $t_b = 1.34 \pm 0.60$ days, $k = 0.86 \pm 0.14$, and $dt = -6.7 \pm 5.2$ days with $\chi^2/\text{d.o.f.} = 0.74$. As before, the parameter n was fixed at $n = 10$ (Figs. 12, 13). The fact that α_2 is less-well determined when we include the data points obtained after day 10 is not surprising. It is basically due to the lack of data between day 4 and 10 combined with the early and rapidly dominating SN component that makes the error of the deduced α_2 relatively large. This is also the reason why in Tab. 6, where we discuss the appropriate afterglow model, we used the fitting results obtained for those data when the SN component is still negligible.

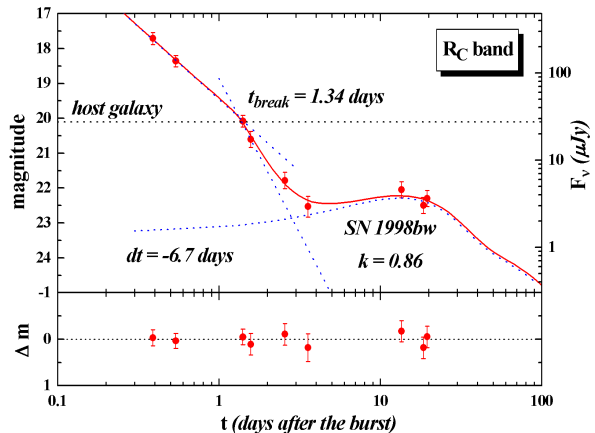


Fig. 12.— The same as Fig. 8 but with dt (eq. 2) as a further free parameter.

The fit improves after inclusion of published late-time HST data (Bloom et al. 2002). With these additional data we find for the R -band light curve: $\alpha_1 = 1.66 \pm 0.44$, $\alpha_2 = 3.43 \pm 0.68$, $t_b = 1.33 \pm 0.48$ days, $k = 0.96 \pm 0.06$, and $dt = -5.1 \pm 1.85$ days with $\chi^2/\text{d.o.f.} = 0.60$ (Figs. 14). Finally, if we follow section 3.2.1 and include the transformed H -band data point and the early-time data from Garnavich et al (2003) we get basically the same result with slightly reduced error bars for α_1 and t_b .

It was already previously noted (Bloom et al. 2002) that a negative time delay dt (Eq. 2) of order of a few days provides a better fit to the data than setting $dt = 0$ days, i.e. GRB and SN start at the same time. Basically, two scenarios could explain such a delay. First, this phenomenon could be intrinsic to the ejected supernova shell itself in the sense that light curve shapes of type Ibc/II supernovae are a function of the mass of the progenitor and other details of the explosion (as already remarked by Bloom et al. 2002). The more exciting alternative is that this delay could point to a genuine time delay between the supernova explosion (formation of a neutron star) and the GRB (interpreted as the subsequent formation of a black hole; see Vietri & Stella 2000). It is tempting to use the negative delay found in our fitting procedure as an argument in support of the supranova model (Vietri & Stella 2000). However, it is worth to remember that the supranova model requires

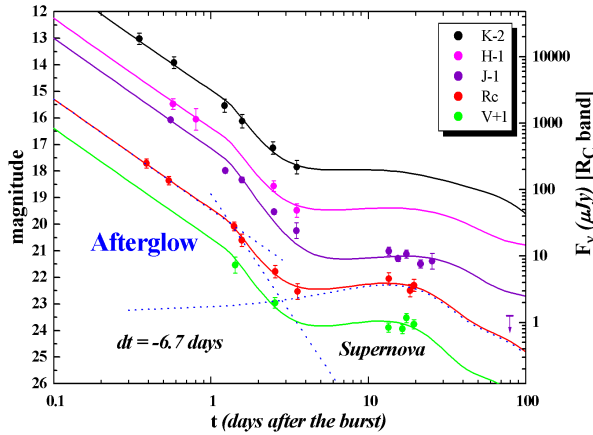


Fig. 13.— The same as Fig. 9 but for $dt = -6.7$ days.

a delay between the supernova and the GRB of many weeks to months (Vietri & Stella 2000), not days. If this delay is shortened, then the original goal of the model, namely to explain the long-lived iron lines, is dismissed. Much better data on both the GRB afterglow and the SN light curve are required to establish the reality of such an offset. GRB 011121 has not been sampled enough to allow rigorous statements about the temporal relationship between SN and GRB, and the use of SN1998bw as a template is also a rather unreliable assumption of our modeling, as pointed out above, and further discussed below.

4.2.3. Alternative explanations for extra light

We note that there are three observational details that do not fit the generally used template SN 1998bw:

1. Rapid intensity decay: The J -band flux on 9 February 2002 is far below the prediction of SN 1998bw. While there exist supernovae with rapidly decaying light curves, this faster decline applies only for times $t > 80$ days. These supernovae are thought to possibly produce less Ni, but more Ti. In the case of GRB 011121, the observed faster decay happened within less than 60 days after the maximum, and thus cannot be explained with a low Ni production.
2. Atypical color evolution: SN decay slower

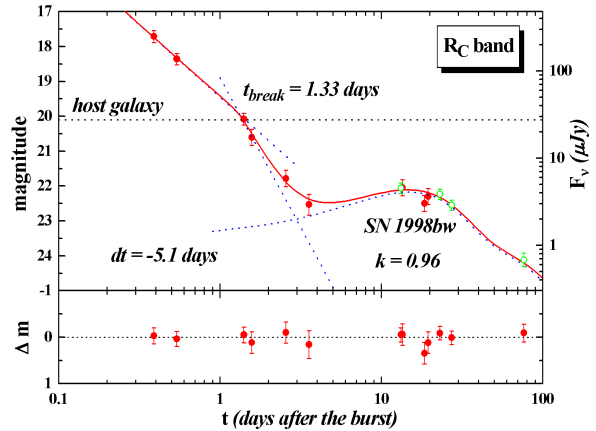


Fig. 14.— The same as Fig. 12 but with the inclusion of published HST R -band data from Bloom et al. (2002).

at longer wavelength, e.g., SN 1998bw or SN 2002ap. The light curve of GRB 011121 shows that the brightness decay in the J band is very rapid. Moreover, the HST data demonstrate that the decay in the R band is not only slower than that in the J band, but also the V -band decay is slower than the R -band decay. Thus, in GRB 011121 the color dependence is just inverted relative to a supernova: the longer the wavelength, the faster the decay.

3. Different spectral energy distribution: The excess light in GRB 011121 is substantially bluer than that of SN 1998bw, as already noted by Garnavich et al. (2003). This is most easily recognized in the different k values for the different filters: while $k = 0.86 \pm 0.14$ for the R_c band (see previous section; excluding the HST data), we find $k = 1.10 \pm 0.50$ in the V band and $k = 0.40 \pm 0.03$ in the J band.

We investigated the alternative to the supernova interpretation, namely a dust echo due to scattered light (Esin & Blandford 2000; Waxman & Draine 2000; Reichart 2001). In the absence of extinction within the host galaxy, as in the case of GRB 011121, the dust echo is expected to be bluer than prescattered light, just as observed. This would suggest that a thermal dust echo is clearly

ruled out since it would peak in the near-infrared band (Reichart 2001). However, in the dust echo scenario there seems to be a severe problem with the temporal evolution. Dust echoes due to scattered light do not peak as sharply as thermal dust echoes or supernovae (Reichart 2001). The time dependence comes from the angular dependence of the escape probability of the scattered photons. Using the values of the differential escape probability as presented by Esin & Blandford (2000), we find that the inferred temporal decay should be much smaller than the observed decay rate after the bump maximum. Other alternatives are neutrons in the blast wave (Beloborodov et al. 2003), the scenario of a refreshed relativistic shock in the GRB outflow caused by the wind profile of the GRB progenitor (Ramirez-Ruiz et al. 2001), the shell collision model (Kumar & Piran 2000) or continuous injection (Björnsson et al. 2002). However, these scenarios are not yet detailed enough to be tested against observational data.

4.3. The break in the light curve

One might be concerned that the break in the R band light curve happens at an intensity level which just corresponds to the R band brightness of the host. However, this is chance coincidence, and only applies to the R band. There are three arguments in favor of the break being unaffected by the host brightness: (1) A subtraction of a constant flux could potentially produce a jump in the light curve, but no break with increasing deviation at later times. (2) The R band brightness of the host is the brightness integrated over the area of the host. In contrast, the additional flux which the host would add to the PSF area of the afterglow is at least a factor of 4 smaller. Thus, if the break would have been “produced” by a wrong host subtraction, it would occur at a level nearly 2 magnitudes fainter. (3) The brightness of the host is different in different filter bands ($V - J = 1.3$ mag). This color is different than that of the afterglow ($V - J = 2.45$ mag; both values not corrected for extinction). Yet, the break is found at the same *time* in *all* filter bands, irrespective of the relative brightness of the host to the afterglow.

The break time t_b we deduce has an 1σ error of 0.5 days so that one might tentatively conclude that any break occurred between about 1 and 2 days after the burst. Whereas a break at very

early times ($t < 1$ day) is excluded by the data obtained by Price et al. (2002) and Garnavich et al. (2003), a break at $t = 2 - 3$ days could be hidden by the bright SN component. The following discussion relies on the deduced break time of $t_b \approx 1.3$ days.

According to Livio & Waxman (2000), for a jetted explosion into a wind-blown surroundings with an $n(r) \sim r^{-2}$ gas density profile it is

$$\Theta_{\text{jet}} \approx 0.11 \left(\frac{E_{53}}{\dot{M}_{-5}/v_{w,3}} \right)^{-1/4} \left(\frac{t_b}{1+z} \right)^{1/4}, \quad (3)$$

where \dot{M}_{-5} is the mass loss rate of the star in units of $10^{-5} M_{\odot} \text{ yr}^{-1}$, $v_{w,3}$ is the wind velocity in units of 10^3 km s^{-1} and E_{53} is the isotropic equivalent energy of the fireball in units of 10^{53} erg. We introduced a factor $(1+z)$ in order to correct for the redshift. Using $z=0.36$, $E_{53}=0.27$ and assuming $\dot{M}_{-5}/v_{w,3} = 1$ we obtain $\Theta_{\text{jet}} \sim 9^\circ$. This corresponds to a beaming factor ($b \approx 2/\Theta_{\text{jet}}^2$) of about 100.

Usually it is assumed that E_{53} can be approximated by the isotropic equivalent energy release E_{γ} in the gamma-ray band during the burst phase. According to Garnavich et al. (2003), for GRB 011121 it was $E_{\gamma} = 0.27 \times 10^{53}$ erg (see also §3.4). After correcting for the beaming factor this gives an energy release of about 3×10^{50} erg, in agreement with the typical energy releases of GRBs (Frail et al. 2001).

Given the many multi-filter observations during the first 4 days (Tab. 1), we have constructed broad-band spectra from the optical to the near-infrared region. These are shown in Fig. 15 with a separation of about 24 hrs between each other. The spectral energy distributions of the first four days are consistent with a $\beta = 0.70$ power-law. This suggests that the break in the light curve was achromatic, in agreement with the predictions of the jet model. We note in passing that we do not see β to evolve towards an asymptotic value of 1.1 as has been argued by Dado et al. (2002b) and assumed for the cannonball interpretation of the GRB 011121 afterglow light curve.

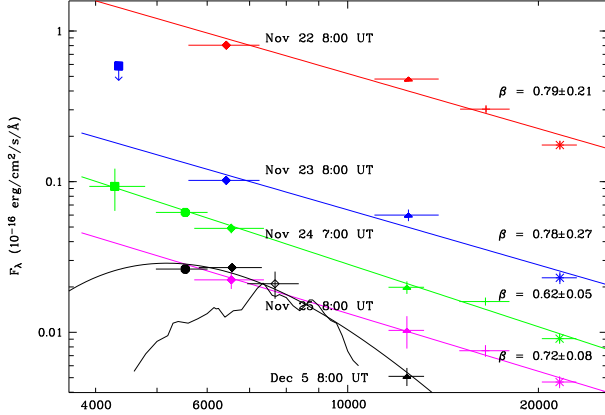


Fig. 15.— Extinction-corrected, broad-band spectral energy distribution of GRB 011121 on four consecutive days, starting about 14 hrs after the GRB, and on 5 December 2001 near the maximum of the supernova-bump. The best-fit power law slopes β are given at the right side except for December 5. The maximum deviation of the data to the power law is ~ 0.15 mag, justifying the systematic error added in the light curve fitting procedure. It can be seen that the spectral slope does not change over the first four days, supporting the jet nature of the break seen in the light curve. The December 5 (filled circles) spectrum is clearly not of power law type. The smooth solid curve is a blackbody with a temperature of 6300 K, while the thin solid line is the spectrum of SN 1998bw, redshifted to $z=0.36$. Note that on Nov. 24, approximately 1 day after the break, the value of β is well-defined and within the error bars well consistent with the predictions of the jet-wind model (Table 6; case 2).

4.4. The host galaxy

4.4.1. Morphology

Images in R , V , and J show that the host galaxy starts affecting the brightness estimate of the afterglow already after November 24, 2001. We have therefore taken the J -band image from February 9 to model the shape and intensity distribution of the host galaxy in order to subtract the host flux from the earlier images. The February 9 exposure consists of two sub-exposures, each with 30 min exposure time, and taken at a mean seeing of $0''.45$ and $0''.55$, respectively. We used the

$0''.45$ part and modelled the host galaxy using a bulge component

$$I_{\text{bulge}}(R) = I_{\text{bulge},0} \exp \left[-7.67 \left(\frac{R}{R_e} \right)^{1/4} \right] \quad (4)$$

and a disk component

$$I_{\text{disk}}(R) = I_{\text{disk},0} \exp \left(-1.68 \frac{R}{R_e} \right). \quad (5)$$

For each of these two components, the four parameters $I_{\text{bulge},0}$, ($I_{\text{disk},0}$), effective radius R_e , position angle (PA) and eccentricity ($e = \sqrt{1 - (b/a)^2}$) are derived using the IRAF/SPP package GIM2D (Simard 1998). The resulting fit parameters are:

- Bulge component: $I_{\text{bulge},0} = 14.78$ mag/arcsec², $R_e = 5.0$ pixel, $e = 0.19$, PA = -41°
- Disk component: $I_{\text{disk},0} = 22.18$ mag/arcsec², $R_e = 19.5$ pixel, $e = 0.19$, PA = -46° .

The eccentricity derived from the galaxy profile in the J band corresponds to an inclination of ~ 10 degrees.

The fit to the radial profile is given in Fig. 16. To subtract the host galaxy emission from the images taken in November/December 2001, this model of the host galaxy was convolved with the corresponding seeing of each image, and then subtracted. For filters other than J , the total brightness of the model was modified to achieve good subtraction in the corresponding band, i.e. the normalization was varied to minimize the residuals. Aperture photometry on the subtracted images was then applied to obtain the magnitudes of the afterglow (see Tab. 1 and Fig. 9).

Using the model parameters given above, and integrating over the galaxy, we obtain the following apparent magnitudes of the host galaxy: $J = 19.1 \pm 0.1$, $R = 20.1 \pm 0.1$, and $V = 20.4 \pm 0.1$.

The decomposition of the surface brightness profile of the galaxy into a disk and a bulge component shows that the bulge dominates within the inner $0''.5$ only. The bulge contributes about 22% to the total light. This can be interpreted as a Sbc morphological type. The observed brightnesses of the host galaxy in the V , R and J band correspond, after correction for foreground absorption and applying the k -correction, to absolute magnitudes of -22.58 ± 0.53 , -22.24 ± 0.24 ,

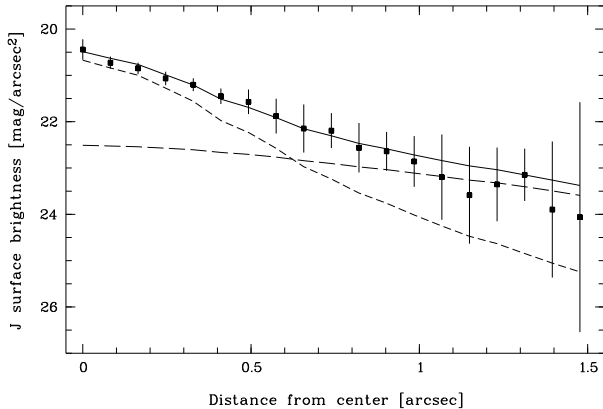


Fig. 16.— Surface brightness profile of the host galaxy of GRB 011121 in the J band, measured on the 2002 February 9 image (first part) at $0''.45$ seeing with a plate scale of $0''.147/\text{pixel}$ (two data points per pixel). The abscissa is the distance from the center measured as $\sqrt{a^2 + b^2}$, with a and b being the major and minor axes of the galaxy. The dashed line denotes the bulge component, the long-dashed line the disk component, and the full line the sum of both components.

and -22.09 ± 0.25 , respectively. This is at the very bright end of the range populated by spirals (e.g., Binggeli et al. 1988); the host galaxy of GRB 011121 is thus among the brightest 5% Sbc galaxies.

The gamma-ray burst happened at an offset of $0''.9$ from the center of the host galaxy (as measured on a VLT image taken at $0''.6$ seeing), corresponding to a physical distance of 9 kpc (see also Ryder et al. 2001). The above derived disk radius is $R_e = 29$ kpc. This offset location of the gamma-ray burst with its supernova is consistent with the general supernova picture, as well as with offsets found for earlier GRBs (Bloom et al. 2002).

4.4.2. The star-formation rate

Using the extinction corrected line fluxes of [O II] and $H\alpha$ (Tab. 5) and the relations given by Kennicutt (1998), i.e. $\text{SFR} (\dot{M}/\text{yr}) = 1.4 \times 10^{-41} \times L(\text{OII})$ and $\text{SFR} (\dot{M}/\text{yr}) = 7.9 \times 10^{-42} \times L(H\alpha)$, we deduce a star formation rate of $1.2 M_\odot/\text{yr}$ and $0.72/0.61 M_\odot/\text{yr}$, respectively. In contrast, Subrahmanyan et al. (2001) derive a star-formation rate of $13\text{--}70 M_\odot/\text{yr}$ from their radio detection of

the host galaxy at 0.05 mJy and assuming a spectral slope of -0.5 between 1.4 and 8.5 GHz. The rate derived here is at the low end of the range found previously in GRB host galaxies. However, also for these earlier cases different results are obtained for different methods/lines, in particular also a large difference between radio- vs. optically-based data (Vreeswijk et al. 2001).

We have no explanation for the fact that the host galaxy appears to be among the brightest 5% Sbc galaxies, and yet the derived star-formation rate is rather low. Also, the lack of clear evidence for dust in the GRB host along the line of sight is somewhat surprising in the supernova picture, though there is also no strong intrinsic extinction in most previous GRB hosts.

5. Concluding remarks

While our α and β values are consistent within the errors with those reported by Garnavich et al. (2003) and Price et al. (2002), the change in our values due to the discovery of the break and the evolution during the four days after the GRB leads to a preference of the jet-wind model. The observed break and its interpretation is in contradiction with the interpretation of the radio data by Price et al. (2002) suggesting a break at times later than 8 days after the GRB. We cannot offer a solution to this problem, as the break is observationally evident from a dozen of data points spread over several filter bands.

Our observations reveal a light curve break at early times and the appearance of extra light at late times. The former is believed to be evidence for a collimated outflow (a fireball jet), whereas the latter could be due to supernova light. Finally, the $\alpha - \beta$ -relations favor a wind model (Table 6). The afterglow of GRB 011121 thus provides another case in support of the current standard paradigm of long-duration gamma-ray bursts: the collapsar model (Woosley 1993, Hartmann & Woosley 1995) in which the birth of a black hole inside a rapidly rotating massive star is announced via jet formation, breakout, and propagation into a stellar environment that was shaped by the strong winds of the pre-collapse star. In fact, GRB 011121 is the first case, where all three signatures (jet break, wind density profile and supernova bump) have been found, while in earlier

cases only two of these three ingredients could be found (e.g., Jaunsen et al. 2001). However, even with GRB 011121 this line of reasoning remains circumstantial, and many more afterglows have to be observed, and better sampled than is presently the case, to seriously establish the GRB-collapsar picture.

6. Acknowledgments

We are highly indebted to the ESO staff, in particular N. Ageorges, S. Bagnulo, H. Böhnhardt, V. Doublier, O.R. Hainaut, S. Hubrig, A.O. Jaunsen, E. Jehin, R. Johnson, A. Kaufer, M. Kürster, E. Mason, E. Pompei, Th. Szeifert for prompt execution of the observing requests and all the additional effort related to that. We thank the anonymous referee for the extensive comments on the original version of this paper. J. Gorosabel acknowledges the receipt of a Marie Curie Research Grant from the European Commission, and J.M. Castro Cerón the receipt of a FPI doctoral fellowship from Spain's Ministerio de Ciencia y Tecnología. This work was supported by the Danish Natural Science Research Council (SNF), by "IUAP P5/36" Interuniversity Attraction Poles Programme of the Belgian Federal Office for Scientific, Technical and Cultural Affairs, and the Belgian Fund for Scientific Research (FWO). This research has made use of the USNOFS Image and Catalogue Archive operated by the United States Naval Observatory, Flagstaff Station (<http://www.nofs.navy.mil/data/fchpix/>).

REFERENCES

- Andersen M.I., Hjorth J., Pedersen H., Jensen B.L., Hunt L.K., et al. 2000, *A&A* 364, L54
- Beloborodov A.M., 2003, *ApJ* 585, L19
- Benetti S. et al. 1999, *MN* 305, 811
- Bertin E., Arnouts S. 1996, *A&AS* 117, 393
- Beuermann K. et al. 1999, *A&A* 352, L26
- Binggeli B., Sandage A.R., Tammann G.A., 1988, *ARAA* 26, 509,
- Björnsson G., Hjorth J., Jakobsson P., Christensen L., Holland S., 2001, *ApJ* 552, L121
- Björnsson G., et al. 2002, *ApJ* 579, L59
- Bloom J.S., et al. 1999, *Nat* 401, 453
- Bloom J.S., Kulkarni S.R., Price P.A., et al., 2002, *ApJ* 572, L45
- Bloom J.S., Kulkarni S.R., Djorgovski S.G., 2002, *AJ* 123, 1111
- Brown M., Schommer R., Olsen K., Jannuzi B., Dey A., Fruchter A., Rhoads J., 2001, *GCN* 1158
- Cardelly J.A., Clayton G.C. & Mathis J.S., 1989, *ApJ* 345, 245
- Castro-Tirado A.J., Gorosabel J., 1999, *A&AS* 138, 449
- Castro-Tirado A.J., Sokolov V.V., Gorosabel J., et al. 2001, *A&A* 370, 398
- Chevalier R.A., Li Z.-Y., 2000, *ApJ* 536, 195
- Dado S., Dar A., De Rujula A., 2002a, *A&A* 388, 1079
- Dado S., Dar A., De Rujula A., 2002b, *ApJ* 572, L143
- de Jong R.S., 1996, *A&A* 313, 45
- Devillard N., 2002, *Eclipse Users Guide*, at URL www.eso.org/projects/aot/eclipse/eug/eug.html
- Dickey J.M., Lockman F.J., 1990, *ARAA* 28, 215
- Drory N., 2003, *A&A* 397, 371
- Esin A. A., Blandford R., 2000, *ApJ* 534, L151
- Frail, D. A. et al. 2001, *ApJ* 562, L55
- Fryer C.L., Woosley S.E., Hartmann D.H., 1999, *ApJ* 526, 152
- Galama, T. J. et al. 1998, *Nature* 395, 670
- Galama, T. J. et al. 2000, *ApJ* 536, 185
- Garnavich P.M., Holland S.T., Jha S., et al., 2001, *GCN* 1273
- Garnavich P.M., Stanek K.Z., Wyrzykowski L., et al., 2003, *ApJ* 582, 924
- Greiner J., Klose S., Zeh A., Lamer G., Scholz R.D., et al., 2001, *GCN* 1166

- Hartmann D.H., Woosley S.E., 1995, *Adv. Space Res.* 15(5), 143
- Heger A., Fryer C.L., Woosley S.E., Langer N., Hartmann D.H., 2003, *ApJ* (subm., astro-ph/0212469)
- Hjorth J., Sollermann J., Moller P., et al. 2003, *Nat.* 423, 847
- Holland S.T., Fynbo J.P.U., Hjorth J., Gorosabel J., Pedersen H. et al., 2001, *A&A* 371, 52
- Holland S.T., Weidinger M., Fynbo J.P.U., Gorosabel J., Hjorth J., Pedersen K., 2003, *AJ* (subm.; astro-ph/0211094)
- Hurley K., Cline T., Guidorzi C., Montanari E., Frontera F., Feroci M., 2001, GCN 1148
- Hurley K., Cline T., Mitrofanov I., Anfimov D., Kozyrev A. et al. 2002, GCN 1372
- Infante L., Garnavich P.M., Stanek K.Z., Wyrzykowski L., 2001, GCN 1152
- Jaunsen, A.O., Hjorth J., Björnsson G., et al. 2001, *ApJ*, 546, 127
- Kennicutt R.C., 1998, *ARAA* 36, 189
- Klose S., Stecklum B., Masetti N., et al. 2000, *ApJ* 545, 271
- Kumar P., Piran T., 2000, *ApJ* 532, 286
- Kumar P., Panaitescu, A. 2000, *ApJ* 541, L9
- Landecker, T. L. et al. 1999, *APJ* 527, 866
- Lazzati D., Covino S., Ghisellini G., Fugazza D., Campana S., et al. 2001, *A&A* 378, 996
- Lazzati D., Rossi E., Covino S., Ghisellini G., Malesani D., 2002, *A&A* 396, L5
- Livio, M., & Waxman, E. 2000, *ApJ*, 538, 187
- Masetti N., Palazzi E., Pian E., et al. 2003, *A&A* 404, 465
- Mészáros P., Rees M.J. & Wijers R.A.M.J. 1998, *ApJ* 499, 301
- Mészáros P., 2002, *ARA&A* 40, 137
- Mitrofanov I., et al. 2003 (in prep)
- Patat F., Cappellaro E., Danziger J., et al. 2001, *ApJ* 555, 900
- Phillips M.M., Krisciunas K., Garnavich P.M., Holland S., Jha S., Stanek K.Z., McCarthy P., 2001, GCN 1164
- Piro L., 2001a, GCN 1147
- Piro L., 2001b, GCN 1149
- Piro L., Soffitta P., Antonelli L.A., in't Zand J., Heise J., et al. 2001, GCN 1172
- Predehl P., Schmitt J.H.M.M., 1995, *A&A* 293, 889
- Price P.A., McCarthy P., Fox D.W., Koviak K., Bloom J.S., 2001, GCN 1153
- Price P.A., Berger E., Reichart D.E., et al., 2002, *ApJ* 572, L51
- Ramirez-Ruiz E., et al. 2001, *MN* 327, 829
- Reichart D.E., 2001, *ApJ* 554, 643
- Rhoads, J. 1999, *ApJ* 525, 737
- Rhoads J.E. & Fruchter A.S., 2001, *ApJ* 546, 117
- Rieke, G.H., Lebofsky, M.J. 1985, *ApJ* 288, 618
- Ryder S., Gunn K., Seymour N., Price P.A., Schmidt B.P., Axelrod T.S., 2001, GCN 1163
- Sari R., Piran T., Narayan R., 1998, *ApJ* 497, L17
- Sari, R., Piran, T., Halpern, R. 1999, *ApJ* 519, L17
- Schlegel, D., Finkbeiner, D., Davis, M. 1998, *ApJ* 500, 525
- Simard L., 1998, in *Astronomical Data Analysis Software and Systems VII*, ASP Conf. Ser. 145, eds. R. Albrecht, R.N. Hook and H.A. Bushouse, p. 108
- Stanek K.Z., Wyrzykowski L., 2001, GCN 1160
- Subrahmanyam R., Kulkarni S.R., Berger E., Frail D.A., 2001, GCN 1156
- Tinney C., Stathakis R., Cannon R., Galama T., 1998, *IAU Circ.* 6896

- van Paradijs J., Groot P.J., Galama, T., et al.,
1997, Nature 386, 686
- van Paradijs J., Kouveliotou C., Wijers R., 2000,
ARAA 38, 379
- Vietri M., Stella M., 1998, ApJ 507, L45
- Vietri M., Stella M., 2000, ApJ 527, L43
- Vreeswijk P.M., Fender R.P., Garrett M.A., Tin-
gay S.J., Fruchter A.S., Kaper L., 2001, A&A
380, L21
- Waxman E., Draine B.T., 2000, ApJ 537, 796
- Wei D.M., Jin Z.P., 2003, A&A 400, 415
- Weiler K.W., Panagia N., Montes M., Sramek, R.
A. 2002, ARAA 40, 387
- Woosley S.E., 1993, ApJ 405, 273
- Wyrzykowski L., Stanek K.Z., 2001, GCN 1154
- Wyrzykowski L., Stanek K.Z., Garnavich P.M.,
2001, GCN 1150
- Zeh A., Klose S., Henden A., Greiner J., 2003,
GCN 2115
- Zeh A., Klose S., 2003, ApJ (submitted)